Hindawi Publishing Corporation
International Journal of Navigation and Observation
Volume 2008, Article ID 813821, 15 pages
doi:10.1155/2008/813821

Research Article

GPS/Reduced IMU with a Local Terrain Predictor in Land Vehicle Navigation

Debo Sun, Mark G. Petovello, and M. Elizabeth Cannon

Position, Location And Navigation (PLAN) Group, Department of Geomatics Engineering, Schulich School of Engineering, University of Calgary, 2500 University Dr. NW, Calgary, AB, Canada T2N 1N4

Correspondence should be addressed to Debo Sun, debsun@ucalgary.ca

Received 18 June 2008; Accepted 3 September 2008

Recommended by Paul Cross

In order to reduce the cost and volume of land vehicle navigation (LVN) systems, a "reduced" inertial measurement unit (IMU) consisting of only one vertical gyro and two or three accelerometers is generally used and is often integrated with other sensors. Since there are no horizontal gyros in a reduced IMU, the pitch and roll cannot be calculated or observed directly from the inertial data, and the navigation performance is thus affected by local terrain variations. In this work, a reduced IMU is integrated with global positioning system (GPS) data and a novel local terrain predictor (LTP) algorithm. The latter is used primarily to help estimate the pitch and roll of the reduced IMU system and thus to improve the navigation performance. In this paper, two reduced IMU configurations and two grades of IMUs are investigated using field data. Test results show that the LTP is valid. Specifically, inclusion of the LTP provides more than an 80% horizontal velocity improvement relative to the case when the LTP is not used in a GPS/reduced IMU configuration.

1. INTRODUCTION

With recent automobile technology development, vehicle safety and control have been given more attention both in civil and military applications. To this end, land vehicle navigation (LVN) plays a critical role and this is evident from the large number of publications on the topic in recent years. Specifically, LVN studies have focused on low-cost micro-electro-mechanical system (MEMS) inertial measurement units (IMUs) [1–4], reduced IMUs [5–11], and on GPS and inertial navigation system (INS) integration [4, 12] to GPS/IMU plus more vehicle sensors integration [2, 3].

In inertial navigation, a full six degree of freedom IMU consists of three orthogonal accelerometers and three orthogonal gyros. The three gyro measurements are used to calculate attitude, and the three accelerometer measurements are used to calculate velocity and position. Gyros are used to measure rotations in space, so the INS always knows the direction in which the accelerometers are pointing [13, 14]. By contrast, in a reduced IMU, where there may be only one vertical gyro, the pitch and roll cannot be measured. Similarly, if fewer than three accelerometers are used, full knowledge of the vehicle's acceleration is unavailable. Both situations introduce errors in the navigation system. This paper focuses on reduced IMUs comprised of two or three accelerometers and one vertical gyro which are typical in LVNs to reduce cost. These configurations are based on the supposition that roads are relatively flat such that horizontal gyros and (in some cases) one vertical accelerometer provide relatively little information [6]. However, in reality, these sensors do provide critical information, and their omission inevitably degrades the performance of the navigation system.

In order to overcome the disadvantages of reduced IMUs, integrating reduced IMUs with other navigation systems or constraints is a means of improving performance; for example, GPS/reduced IMU [6, 7] and GPS/reduced IMU with vehicular constraints [5]. To this end, since many new model vehicles are already equipped with GPS receivers and some newer vehicles also contain reduced IMUs, integrating the two systems provides the opportunity for a minimal cost land vehicle navigation system. Such a system can also provide a base for other (augmented) integration strategies. For example, integrating a GPS/reduced IMU with other

vehicular sensors such as a wheel speed sensor can be considered as a hardware-based augmentation method. Conversely, vehicle dynamic constraints such as nonholonomic constraints provide a software-based augmentation option (e.g., [5]). Although hardware augmentations can be used to improve navigation performance, they can increase the cost of an LVNS if additional vehicular sensors need to be installed in the vehicle. Software methods are popular because they do not require hardware to be installed, thus reducing cost.

The local terrain predictor method presented in this paper is a form of software augmentation. It can be envisaged as an error modeling method for reduced IMUs that compensates for terrain-induced roll and pitch variations. It does not increase the measurement variables of GPS/reduced IMU, but only changes the navigation equation and error model of the reduced IMU.

For GPS/reduced IMU systems with an LTP, if GPS is available, the local terrain (or equivalently, the pitch and roll) can be estimated. Once the local terrain is modeled, the terrain model can be used to predict the pitch and roll in an attempt to improve performance relative to the case where the pitch and roll are assumed zero. This prediction applies to both the case when GPS is continually available and when GPS is unavailable. In the latter case, the terrain effects are assumed to be constant over time.

The proposed algorithm is evaluated using real data collected with both a tactical-grade and MEMS-grade IMU and different reduced IMU sensor configurations. In particular, two kinds of reduced IMU configurations are considered; a three accelerometer and one vertical gyro (3A1G) configuration; and a two horizontal accelerometers and one vertical gyro (2A1G) configuration. System performance in the absence of GPS data is also evaluated.

The paper begins with a derivation of the navigation equations and the corresponding error model of the reduced IMU. During the derivation, the local terrain model is established and integrated into the error model. Then the field test and data analysis procedures are described followed by an analysis of the results. Finally, conclusions are drawn based on the results presented.

2. MECHANIZATION OF A REDUCED IMU

There are many different reduced IMU configurations [5], but for land vehicle navigation, there are only a few which are practical such as 3A1G and 2A1G as previously described. In the following, first, the relevant coordinate systems are described, then the derivation of the mechanization and corresponding error model of the reduced IMU is given based on a 3A1G configuration, and finally the mechanization and corresponding error model of a 2A1G configuration are obtained.

2.1. Coordinate systems

The coordinate systems used in this paper are as follows:

(i) inertial frame (i-frame),

(ii) earth-fixed frame (e-frame),

(iii) local level frame (ℓ-frame),

(iv) body frame (b-frame), and

(v) alternative level frame ($\ell 1$-frame).

The i-frame is a fixed coordinate with the center of the Earth as its origin. Its z axis is parallel to the spin axis of the Earth, x points to the mean vernal equinox, and y is determined by x and z in a right-handed system. The e-frame coincides with the i-frame at the origin but rotates with the Earth rate. Its z axis is parallel to the z axis of the i-frame, x points to the mean meridian of Greenwich, and y is determined by x and z in a right-handed system. The ℓ-frame is an east, north, up rectangular coordinate system, which is called ENU. The b-frame is rigidly attached to the vehicle of interest, usually at a fixed point such as the center of gravity. The x, y, and z axes of the b-frame, respectively, point in the right, forward, and up directions. The $\ell 1$-frame is another local level frame which has the same origin and vertical axis with those of ℓ-frame, but the directions of other two axes (x and y) are determined by the directions of the corresponding two axes (x and y) of the b-frame.

2.2. Reduced IMU mechanization equations and error model

In the following, the derivation of mechanization equations and error model is based on the 3A1G configuration in which the acceleration information is complete, but the rotation information is incomplete.

2.2.1. Mechanization equations

The navigation equations for the 3A1G can be derived from the equations of motion for a full IMU as shown in (A.1) in the Appendix. Furthermore, only the attitude equation needs to be derived, as below. For details on notation, please refer to the Appendix.

First, from the direction cosine matrix (from b-frame to ℓ-frame):

$$\mathbf{R}_b^\ell = \mathbf{A}_z(\psi)\mathbf{A}_x(-p)\mathbf{A}_y(-r), \tag{1}$$

where ψ is azimuth, p is pitch, r is roll, $\mathbf{A}_j(\bar{\omega})$, $j = x, y, z$, $\bar{\omega} = p, r, \psi$, is a rotation matrix about j-axis by angle $\bar{\omega}$. Taking the derivative of (1), the following equation can be obtained:

$$\dot{\mathbf{R}}_b^\ell = \dot{\psi}\dot{\mathbf{A}}_z(\psi)\mathbf{A}_x(-p)\mathbf{A}_y(-r) + \dot{p}\mathbf{A}_z(\psi)\dot{\mathbf{A}}_x(-p)\mathbf{A}_y(-r) + \dot{r}\mathbf{A}_z(\psi)\mathbf{A}_x(-p)\dot{\mathbf{A}}_y(-r), \tag{2}$$

where $\dot{\mathbf{A}}_z(\psi) = d\mathbf{A}_z(\psi)/d\psi$, $\dot{\mathbf{A}}_x(-p) = d\mathbf{A}_x(-p)/dp$, and $\dot{\mathbf{A}}_y(-r) = d\mathbf{A}_y(-r)/dr$.

Premultiplying both sides of (2) by $\mathbf{A}_z(-\psi)$ yields

$$\mathbf{A}_z(-\psi)\dot{\mathbf{R}}_b^\ell = \dot{\psi}\mathbf{A}_z(-\psi)\dot{\mathbf{A}}_z(\psi)\mathbf{A}_x(-p)\mathbf{A}_y(-r) + \dot{p}\dot{\mathbf{A}}_x(-p)\mathbf{A}_y(-r) + \dot{r}\mathbf{A}_x(-p)\dot{\mathbf{A}}_y(-r). \tag{3}$$

From the rotation matrices and their derivatives, the following equations are obtained:

$$\dot{\mathbf{A}}_x(-p)\mathbf{A}_x(p) = \begin{bmatrix} 0 & 0 & 0 \\ 0 & 0 & -1 \\ 0 & 1 & 0 \end{bmatrix},$$
$$\dot{\mathbf{A}}_y(-r)\mathbf{A}_y(r) = \begin{bmatrix} 0 & 0 & 1 \\ 0 & 0 & 0 \\ -1 & 0 & 0 \end{bmatrix}, \quad (4)$$
$$\mathbf{A}_z(-\psi)\dot{\mathbf{A}}_z(\psi) = \begin{bmatrix} 0 & 1 & 0 \\ -1 & 0 & 0 \\ 0 & 0 & 0 \end{bmatrix}.$$

Postmultiplying (3) with $\mathbf{A}_y(r)\mathbf{A}_x(p)$ and substituting (4), the following is obtained:

$$\mathbf{A}_z(-\psi)\dot{\mathbf{R}}_b^{\ell}\mathbf{A}_y(r)\mathbf{A}_x(p) = \begin{bmatrix} 0 & \dot{\psi} - \dot{r}\sin p & \dot{r}\cos p \\ -\dot{\psi} + \dot{r}\sin p & 0 & -\dot{p} \\ -\dot{r}\cos p & \dot{p} & 0 \end{bmatrix} = [\boldsymbol{\Theta}\times], \quad (5)$$

where

$$\boldsymbol{\Theta} = \begin{bmatrix} \dot{p} \\ \dot{r}\cos p \\ -\dot{\psi} + \dot{r}\sin p \end{bmatrix}. \quad (6)$$

From (A.1), $\dot{\mathbf{R}}_b^{\ell} = \mathbf{R}_b^{\ell}(\boldsymbol{\Omega}_{ib}^b - \boldsymbol{\Omega}_{i\ell}^b)$ yielding

$$\mathbf{A}_z(-\psi)\dot{\mathbf{R}}_b^{\ell}\mathbf{A}_y(r)\mathbf{A}_x(p) = \mathbf{A}_z(-\psi)\mathbf{R}_b^{\ell}(\boldsymbol{\Omega}_{ib}^b - \boldsymbol{\Omega}_{i\ell}^b)\mathbf{A}_y(r)\mathbf{A}_x(p). \quad (7)$$

Substituting (1) into (7) gives

$$\mathbf{A}_z(-\psi)\dot{\mathbf{R}}_b^{\ell}\mathbf{A}_y(r)\mathbf{A}_x(p) = \mathbf{A}_x(-p)\mathbf{A}_y(-r)(\boldsymbol{\Omega}_{ib}^b - \boldsymbol{\Omega}_{i\ell}^b)\mathbf{A}_y(r)\mathbf{A}_x(p). \quad (8)$$

According to the definition of $\ell 1$-frame, the following is obtained:

$$\mathbf{R}_b^{\ell 1} = \mathbf{A}_x(-p)\mathbf{A}_y(-r) = \mathbf{A}_z(-\psi)\mathbf{R}_b^{\ell}. \quad (9)$$

With (9), (8) is changed as follows:

$$\mathbf{A}_z(-\psi)\dot{\mathbf{R}}_b^{\ell}\mathbf{A}_y(r)\mathbf{A}_x(p) = \mathbf{R}_b^{\ell 1}(\boldsymbol{\Omega}_{ib}^b - \boldsymbol{\Omega}_{i\ell}^b)\mathbf{R}_{\ell 1}^b = \boldsymbol{\Omega}_{ib}^{\ell 1} - \boldsymbol{\Omega}_{i\ell}^{\ell 1} = [(\boldsymbol{\omega}_{ib}^{\ell 1} - \boldsymbol{\omega}_{i\ell}^{\ell 1})]. \quad (10)$$

Comparing (5) and (10), we obtain

$$\boldsymbol{\Theta} = (\boldsymbol{\omega}_{ib}^{\ell 1} - \boldsymbol{\omega}_{i\ell}^{\ell 1}). \quad (11)$$

With (9), the following can be obtained:

$$\boldsymbol{\omega}_{ib}^{\ell 1} = \mathbf{R}_b^{\ell 1}\boldsymbol{\omega}_{ib}^b = \mathbf{A}_x(-p)\mathbf{A}_y(-r)\begin{bmatrix} \omega_{ibx}^b \\ \omega_{iby}^b \\ \omega_{ibz}^b \end{bmatrix} = \begin{bmatrix} \omega_{ibx}^b\cos r + \omega_{ibz}^b\sin r \\ \omega_{ibx}^b\sin p\sin r + \omega_{iby}^b\cos p - \omega_{ibz}^b\sin p\cos r \\ -\omega_{ibx}^b\cos p\sin r + \omega_{iby}^b\sin p + \omega_{ibz}^b\cos p\cos r \end{bmatrix},$$
$$\boldsymbol{\omega}_{i\ell}^{\ell 1} = \mathbf{A}_z(-\psi)\boldsymbol{\omega}_{i\ell}^{\ell} = \mathbf{A}_z(-\psi)\begin{bmatrix} \omega_{i\ell x}^{\ell} \\ \omega_{i\ell y}^{\ell} \\ \omega_{i\ell z}^{\ell} \end{bmatrix} = \begin{bmatrix} \omega_{i\ell x}^{\ell}\cos\psi - \omega_{i\ell y}^{\ell}\sin\psi \\ \omega_{i\ell x}^{\ell}\sin\psi + \omega_{i\ell y}^{\ell}\cos\psi \\ \omega_{i\ell z}^{\ell} \end{bmatrix}. \quad (12)$$

Substituting (12), and the standard expression for the turn rate $\boldsymbol{\omega}_{i\ell}^{\ell}$ with velocity components v_e, v_n, meridian radius M, prime vertical radius N, height h, latitude φ, and rotation rate of the earth ω_e, into (11), we get the following:

$$\dot{p} = \omega_{ibx}^b\cos r + \omega_{ibz}^b\sin r - \left(\left(\frac{-v_n}{M+h}\right)\cos\psi - \left(\frac{v_e}{N+h} + \omega_e\cos\varphi\right)\sin\psi\right),$$
$$\dot{r}\cos p = \omega_{ibx}^b\sin p\sin r + \omega_{iby}^b\cos p - \omega_{ibz}^b\sin p\cos r - \left(\left(\frac{-v_n}{M+h}\right)\sin\psi + \left(\frac{v_e}{N+h} + \omega_e\cos\varphi\right)\cos\psi\right),$$
$$-\dot{\psi} + \dot{r}\sin p = -\omega_{ibx}^b\cos p\sin r + \omega_{iby}^b\sin p + \omega_{ibz}^b\cos p\cos r - \left(\frac{v_e\tan\varphi}{N+h} + \omega_e\sin\varphi\right). \quad (13)$$

Therefore, the azimuth rate equation is obtained from (13) as

$$\dot{\psi} - \dot{r}\sin p = \omega_{ibx}^b\cos p\sin r - \omega_{iby}^b\sin p - \omega_{ibz}^b\cos p\cos r + \left(\frac{v_e\tan\varphi}{N+h} + \omega_e\sin\varphi\right). \quad (14)$$

From (13), it can be seen that since ω_{ibx}^b and ω_{iby}^b are unknown, pitch and roll cannot be calculated. Because pitch and roll are generally small in land vehicle applications, they can be considered as error terms and will, therefore, be modelled accordingly. However, for the mechanization equations, they are assumed to be zero $p = 0, r = 0$. With this assumption, the azimuth rate equation and attitude direction cosine matrix can be written as

$$\dot{\psi} = -\omega_{ibz}^b + \left(\frac{v_e\tan\varphi}{N+h} + \omega_e\sin\varphi\right), \quad \mathbf{R}_b^{\ell} = \mathbf{A}_z(\psi). \quad (15)$$

Substituting (15) into (A.1), the navigation equations of reduced IMU (3A1G), see (31), are obtained.

2.2.2. Error model

The corresponding error model of the reduced IMU (3A1G) needs to be derived from (A.2) (see the Appendix). Its position error model and accelerometer bias model are the same as those of (A.2), but the other error state models (i.e., velocity, attitude, and gyro biases) are derived in the following.

First, the attitude error model is derived. Recall that in (15), the pitch and roll are assumed to be zero and considered as error terms. However, the pitch and roll are determined by the local terrain and since this terrain can be expressed as a first-order Gaussian Markov process [15], the pitch and roll can also be expressed as first-order Gaussian Markov processes:

$$\begin{aligned} \dot{p} &= -\alpha_p p + w_p, \\ \dot{r} &= -\alpha_r r + w_r, \end{aligned} \tag{16}$$

where α_p, α_r are the inverse of correlation time of the process, and w_p, w_r are driving noise terms.

The definition of the azimuth error is

$$\delta\dot{\psi} = \dot{\tilde{\psi}} - \dot{\psi}, \tag{17}$$

where $\dot{\psi}$ is the "true" azimuth rate which can be obtained from (14), $\dot{\tilde{\psi}}$ is azimuth rate with error and can be obtained from (15). Accordingly,

$$\dot{\tilde{\psi}} = -\tilde{\omega}^b_{ibz} + \left(\frac{\tilde{v}_e \tan\tilde{\varphi}}{\tilde{N}+\tilde{h}} + \omega_e \sin\tilde{\varphi}\right), \tag{18}$$

where $\tilde{\omega}^b_{ibz}$ is the vertical gyro measurement, $\tilde{v}_e, \tilde{\varphi}, \tilde{h}$ are the calculated east velocity, latitude, and height, and $\tilde{N}$ is the calculated prime vertical radius of the reference ellipsoid.

Let

$$\tilde{\omega}^b_{ibz} = \omega^b_{ibz} - d_z, \tag{19}$$

where d_z is the drift of vertical gyro. Since the second term on the right-hand side of (18) is very small, especially relative to the first term, the following approximation is made:

$$\left(\frac{v_e \tan\varphi}{N+h} + \omega_e \sin\varphi\right) - \left(\frac{\tilde{v}_e \tan\tilde{\varphi}}{\tilde{N}+\tilde{h}} + \omega_e \sin\tilde{\varphi}\right) \approx 0. \tag{20}$$

Substituting (14) and (18) into (17) and applying (20), we obtain

$$\begin{aligned} \delta\dot{\psi} \approx{}& -\dot{r}\,\sin p - \omega^b_{ibx}\cos p\,\sin r + \omega^b_{iby}\sin p + d_z \\ &+ (\cos p\,\cos r - 1)\omega^b_{ibz}. \end{aligned} \tag{21}$$

Since ω^b_{ibx}, ω^b_{iby}, and $\dot{r}$ are unknown and since pitch and roll are small, so the terms $\dot{r}\sin p$, $\omega^b_{ibx}\cos p\sin r$, and $\omega^b_{iby}\sin p$ are small values and considered as noise. For the term $(\cos p\,\cos r - 1)\omega^b_{ibz}$, since pitch and roll are only a few degrees, $\cos p\,\cos r - 1 \approx -(p^2 + r^2)/2$ is smaller and, in most cases, ω^b_{ibz} is a few degrees per second, so $(\cos p\,\cos r - 1)\omega^b_{ibz}$ is also small value and considered as noise in order to simplify calculation. Therefore, the sum of the above small terms is approximated as white noise, and the azimuth error model can be approximately expressed as

$$\delta\dot{\psi} \approx d_z + w_\psi, \tag{22}$$

where w_ψ is the equivalent white noise of approximation error of (22) and in general cases, d_z can be expressed as a first-order Gaussian Markov process (e.g., [12]):

$$\dot{d}_z = -\alpha_d d_z + w_d, \tag{23}$$

where α_d is the inverse of the correlation time, w_d is the driving noise, and (23) is determined by the expression of vertical gyro drift.

In order to express the attitude error $\boldsymbol{\varepsilon}^{\ell 1}$ with respect to the pitch, roll, and azimuth errors, the relationship between $\boldsymbol{\varepsilon}^{\ell 1}$ and these errors first needs to be determined. The attitude error can be written as follows [16]:

$$\boldsymbol{\varepsilon}^b = \delta\boldsymbol{\omega}^b_{\ell b} = \begin{bmatrix} \delta\omega^b_{\ell bx} & \delta\omega^b_{\ell by} & \delta\omega^b_{\ell bz} \end{bmatrix}^T. \tag{24}$$

Premultiplying both sides of (24) by $\mathbf{R}^{\ell 1}_b$ yields

$$\boldsymbol{\varepsilon}^{\ell 1} = \delta\boldsymbol{\omega}^{\ell 1}_{\ell b} = \begin{bmatrix} \delta\omega^{\ell 1}_{\ell bx} & \delta\omega^{\ell 1}_{\ell by} & \delta\omega^{\ell 1}_{\ell bz} \end{bmatrix}^T. \tag{25}$$

Perturbing (11), we obtain

$$\delta\boldsymbol{\Theta} = \delta\boldsymbol{\omega}^{\ell 1}_{ib} - \delta\boldsymbol{\omega}^{\ell 1}_{i\ell} = \delta\boldsymbol{\omega}^{\ell 1}_{\ell b}. \tag{26}$$

Comparing (25) and (26) gives

$$\dot{\boldsymbol{\varepsilon}}^{\ell 1} = \delta\dot{\boldsymbol{\Theta}}. \tag{27}$$

Since p and r are small angles of only a few degrees, and in the navigation equations, p and r are chosen as zero, the following is obtained:

$$\dot{\boldsymbol{\varepsilon}}^{\ell 1} = \delta\dot{\boldsymbol{\Theta}} \approx \begin{bmatrix} \delta\dot{p} \\ \delta\dot{r} \\ -\delta\dot{\psi} \end{bmatrix} = \begin{bmatrix} -\dot{p} \\ -\dot{r} \\ -\delta\dot{\psi} \end{bmatrix}. \tag{28}$$

From (16), (22), and (28), the attitude error model can be written as

$$\begin{bmatrix} \dot{\varepsilon}^{\ell 1}_x \\ \dot{\varepsilon}^{\ell 1}_y \\ \dot{\varepsilon}^{\ell 1}_z \end{bmatrix} = \begin{bmatrix} -\alpha_p & 0 & 0 \\ 0 & -\alpha_r & 0 \\ 0 & 0 & 0 \end{bmatrix} \begin{bmatrix} \varepsilon^{\ell 1}_x \\ \varepsilon^{\ell 1}_y \\ \varepsilon^{\ell 1}_z \end{bmatrix} + \begin{bmatrix} 0 \\ 0 \\ -1 \end{bmatrix} d_z + \begin{bmatrix} w_p \\ w_r \\ w_\psi \end{bmatrix}. \tag{29}$$

The velocity error model can be obtained from (A.2) as follows:

$$\delta\dot{\mathbf{v}}^\ell = \mathbf{B}\delta\mathbf{v}^\ell - \mathbf{F}^\ell\boldsymbol{\varepsilon}^\ell + \mathbf{R}^\ell_b\mathbf{b} = \mathbf{B}\delta\mathbf{v}^\ell - \mathbf{R}^\ell_{\ell 1}\mathbf{F}^{\ell 1}\boldsymbol{\varepsilon}^{\ell 1} + \mathbf{R}^\ell_b\mathbf{b}. \tag{30}$$

Finally, substituting (23), (29), and (30) into (A.2), the error model of reduced IMU (3A1G) (see (32)) is obtained.

2.3. Equation summary for 3A1G configuration

The navigation equations are as follows:

$$\begin{aligned}\dot{\mathbf{r}}^{\ell} &= \mathbf{D}^{-1}\mathbf{v}^{\ell},\\ \dot{\mathbf{v}}^{\ell} &= \mathbf{R}_b^{\ell}\mathbf{f}^b - (2\boldsymbol{\Omega}_{ie}^{\ell} + \boldsymbol{\Omega}_{e\ell}^{\ell})\mathbf{v}^{\ell} + \mathbf{g}^{\ell},\\ \dot{\psi} &= -\omega_{ibz}^b + \left(\frac{v_e \tan\varphi}{N+h} + \omega_e \sin\varphi\right),\\ \mathbf{R}_b^{\ell} &= \mathbf{A}_z(\psi),\end{aligned} \tag{31}$$

where ψ is azimuth, $\mathbf{A}_z(\psi)$ is a rotation matrix about the z-axis by angle ψ, and the other variables and parameters have the same definitions as those of a full six degree of freedom IMU; see (A.1).

The corresponding error model is given by

$$\begin{bmatrix}\delta\dot{\mathbf{r}}^{\ell}\\ \delta\dot{\mathbf{v}}^{\ell}\\ \dot{\boldsymbol{\varepsilon}}^{\ell 1}\\ \dot{d}_z\\ \dot{\mathbf{b}}\end{bmatrix} = \begin{bmatrix}\mathbf{0}_{3\times3} & \mathbf{D}^{-1} & \mathbf{0}_{3\times3} & \mathbf{0}_{3\times1} & \mathbf{0}_{3\times3}\\ \mathbf{0}_{3\times3} & \mathbf{B} & -\mathbf{R}_{\ell 1}^{\ell}\mathbf{F}^{\ell 1} & \mathbf{0}_{3\times1} & \mathbf{R}_b^{\ell}\\ \mathbf{0}_{3\times3} & \mathbf{0}_{3\times3} & \boldsymbol{\Gamma}_{\varepsilon} & \mathbf{M}_d & \mathbf{0}_{3\times3}\\ \mathbf{0}_{1\times3} & \mathbf{0}_{1\times3} & \mathbf{0}_{1\times3} & -\alpha_d & \mathbf{0}_{1\times3}\\ \mathbf{0}_{3\times3} & \mathbf{0}_{3\times3} & \mathbf{0}_{3\times3} & \mathbf{0}_{3\times1} & -\boldsymbol{\Lambda}\end{bmatrix}\begin{bmatrix}\delta\mathbf{r}^{\ell}\\ \delta\mathbf{v}^{\ell}\\ \boldsymbol{\varepsilon}^{\ell 1}\\ d_z\\ \mathbf{b}\end{bmatrix} + \begin{bmatrix}\mathbf{0}_{3\times1}\\ \mathbf{0}_{3\times1}\\ \mathbf{W}_{\varepsilon}\\ w_d\\ \mathbf{W}_b\end{bmatrix}, \tag{32}$$

where $\mathbf{R}_{\ell 1}^{\ell} = \mathbf{A}_z(\psi)$, $\mathbf{F}^{\ell 1} = \mathbf{R}_b^{\ell 1}[\mathbf{f}^b\times]$ is a skew symmetric matrix. $\boldsymbol{\Gamma}_{\varepsilon} = \mathrm{diag}(-\alpha_p \;\; -\alpha_r \;\; 0)$, α_p, α_r are the inverse of the correlation time of the local terrain (or pitch and roll). $\mathbf{M}_d = [0 \;\; 0 \;\; -1]^T$. $\mathbf{W}_{\varepsilon} = [w_p \;\; w_r \;\; w_{\psi}]^T$, w_p, w_r are driving noise of local terrain, w_{ψ} is the equivalent white noise of approximation error of azimuth error equation. d_z is vertical gyro's drift, α_d is the inverse of correlation time of d_z, and w_d is the driving noise of d_z. Other variables and parameters have the same definition with those in (A.2).

2.4. Mechanization equations and error model of 2A1G configuration

In this configuration, there are two horizontal accelerometers and one vertical gyro. The acceleration information and rotation information are, therefore, both incomplete, and the difference of 2A1G from 3A1G is that in the former the vertical specific force needs to be calculated.

Suppose the specific force can be expressed as $\mathbf{f}^{\ell} = [f_e \;\; f_n \;\; g + \delta f_u]^T$ in the local level frame (ℓ-frame), where g is acceleration due to gravity and δf_u is the vehicle's true vertical acceleration, f_e and f_n are specific forces in east and north, respectively. So in the body frame (b-frame), specific force can be expressed as

$$\begin{aligned}\mathbf{f}^b &= \begin{bmatrix}f_x^b & f_y^b & f_z^b\end{bmatrix}^T = \mathbf{R}_{\ell}^b\mathbf{f}^{\ell}\\ &= \begin{bmatrix}\mathcal{A} & \mathcal{C} & -\cos p \sin r\\ \sin\psi\cos p & \cos\psi\cos p & \sin p\\ \mathcal{B} & \mathcal{D} & \cos p\cos r\end{bmatrix}\mathbf{f}^{\ell},\end{aligned} \tag{33}$$

where $\mathcal{A}$ denotes $\cos\psi\cos r + \sin\psi\sin p\sin r$, $\mathcal{B}$ denotes $\cos\psi\sin r - \sin\psi\sin p\cos r$, $\mathcal{C}$ denotes $-\sin\psi\cos r + \cos\psi\sin p\sin r$, and $\mathcal{D}$ denotes $-\sin\psi\sin r - \cos\psi\sin p\cos r$, so

$$\begin{aligned}f_z^b = {} & f_e(\cos\psi\sin r - \sin\psi\sin p\cos r)\\ & + f_n(-\sin\psi\sin r - \cos\psi\sin p\cos r)\\ & + g\cos p\cos r + \delta f_u\cos p\cos r.\end{aligned} \tag{34}$$

Since pitch, roll, and δf_u are generally small (most of δf_u is less than $g/10$ and behaves like noise, and δf_u is unknown), and in most vehicle navigation applications, f_e and f_n are less than g, (34) can be simplified as

$$f_z^b \approx g\cos p\cos r. \tag{35}$$

Since the approximation error of (35) is related to the local terrain, which is expressed as a first-order Gauss Markov process, the approximation error of (35) is, therefore, expressed as a first-order Gauss Markov process:

$$\dot{b}_z = -\beta_z b_z + w_{fz}, \tag{36}$$

where β_z is the inverse of the correlation time of b_z, and w_{fz} is the driving noise of b_z.

Substituting (35) into (31), the navigation equations of 2A1G are obtained, which have the same form as (31) except that the vertical acceleration in body frame needs to be calculated with (35) and the best available estimates of the pitch p and roll r.

Substituting (36) into (32), the corresponding error model of 2A1G is obtained, which has the same form as (32) except for the vertical accelerometer bias term. Although the vertical accelerometer bias has the same expression in both 3A1G and 2A1G, it has different parameters or meanings in the two error models. In 3A1G, the bias model comes from the actual vertical accelerometer, but in 2A1G, it comes from the vertical acceleration calculation error, which is related to the local terrain.

3. FIELD TEST DESCRIPTION

In order to investigate the validity of the above method, a field vehicle test was conducted in a suburban area of Calgary in October 2007. Data from the field test was collected and stored for postmission processing.

3.1. Field test setup

Two grades of IMUs were used during the field test: a tactical-grade IMU (Honeywell HG1700) and an MEMS-grade IMU (Crista IMU). For the HG1700 IMU, the gyro drift is 1 deg/h, and the accelerometer bias is 1 milli-g [12]. For the Crista IMU, the gyro turn on drift is 2000–5000 deg/h, noise is 200–300 deg/h/$\sqrt{\text{Hz}}$, and the accelerometer turn on bias and noise are 0.3-0.5 m/s^2 and 0.003-0.004 g/$\sqrt{\text{Hz}}$, respectively [17, 18]. In the field test, a NovAtel SPAN system, which contains a NovAtel OEM4 dual-frequency GPS receiver and a Honeywell HG1700 AG11 IMU, was used. The GPS receiver

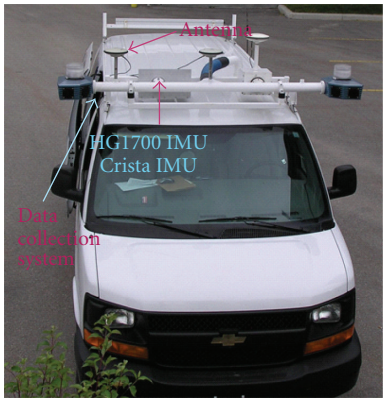

Figure 1: Field test setup.

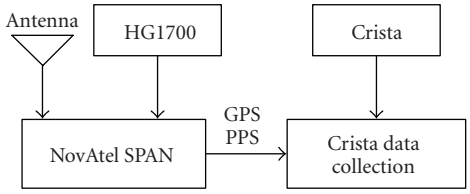

Figure 2: Data collection block diagram.

can provide high-quality code, Doppler, and carrier phase measurements, and the IMU data is time tagged with GPS time thus ensuring synchronicity of the data to better than 1 millisecond. The GPS antennas (one for the SPAN system and another for an unrelated experiment), HG1700 IMU, and Crista IMU were installed on the roof of the test vehicle. Data collection system and power were put inside the vehicle. Figure 1 is the picture of the vehicle setup.

3.2. Data collection

The data collection system is shown in Figure 2. The NovAtel SPAN system provides GPS data and IMU data. For the Crista IMU, the pulse-per-second (PPS) signal from the SPAN system's GPS receiver is used for time tagging purposes. The GPS sampling frequency is 1 Hz, whereas the IMU sampling frequency (for both the HG1700 and Crista) is 100 Hz.

3.3. GPS availability

GPS availability is shown in Figure 3. It can be seen that, in most cases, the number of tracked GPS satellites is seven to nine. Only in a few very short periods, the number of tracked satellites is four to six. As such, it is concluded that there are no naturally occurring GPS outages (<4 SVs) during the field test.

3.4. Trajectory, velocity, and attitude

The field test trajectory is shown in Figure 4, velocity in Figure 5, and attitude in Figure 6. The total vehicle test

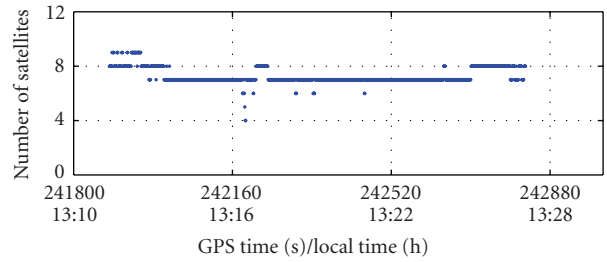

Figure 3: Number of tracked satellites.

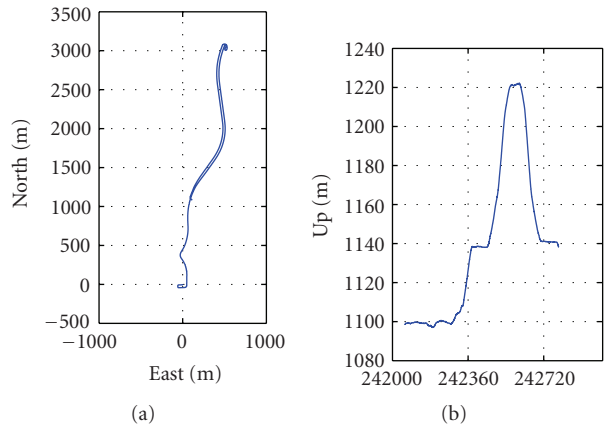

Figure 4: Field test trajectory.

duration is more than 12 minutes. The south-north distance change is about 3 km, and is 500 m in the east-west direction. The vertical variation is more than 100 m. Figure 5 shows the velocity profile with the maximum horizontal velocity being about 25 m/s and the maximum vertical velocity being less than 2 m/s. The reference attitude solution is shown in Figure 6. As expected, the azimuth solution roughly shows the orientation of the road on which the vehicle moves. In contrast, pitch and roll generally show the slope of the road (some vehicle specific attitude variations are also included, but these are expected to be small compared to the terrain variations and have relatively short duration). In the field test, the pitch and roll mostly range between −3 and 3 degrees. The maximum pitch and roll is 4 degrees in each case. The root mean square (RMS) of the pitch and roll is 2.1 degrees. In the following discussion, the term "local terrain" will mean pitch and roll variations only (not azimuth).

The reference solution was obtained using a differential GPS solution integrated with the HG1700 IMU. It is assumed that the reference solution has a similar accuracy level with that in [18], which is also generated using a DGPS/HG1700 IMU system: the RMS of the position error of the reference solution in each direction is about 0.23 m, the RMS of velocity accuracy 0.015 m/s in each direction, and the RMS of attitude accuracy is 0.03 degrees in pitch and roll and 0.17 degrees in azimuth.

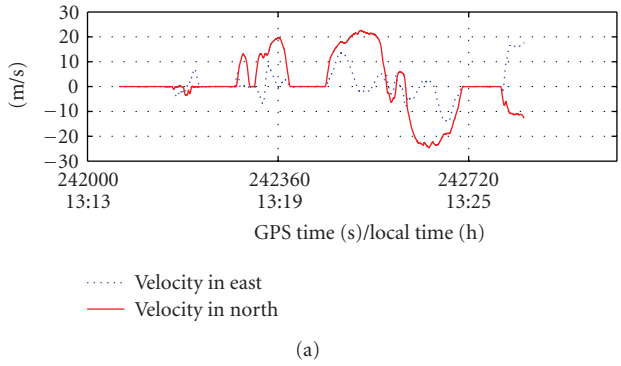

(a)

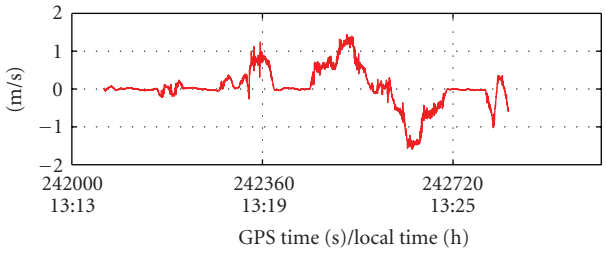

(b)

Figure 5: Field test velocity.

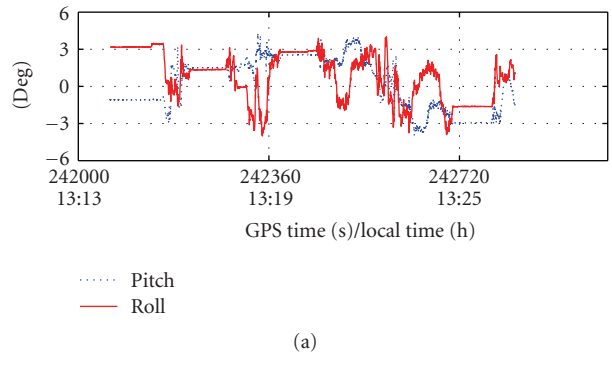

(a)

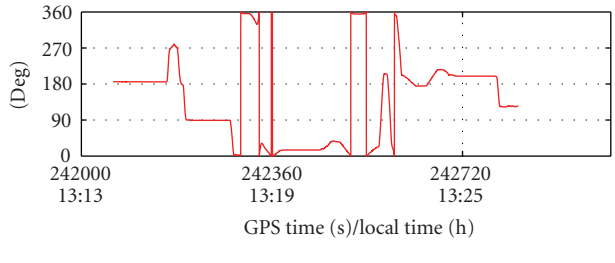

(b)

Figure 6: Reference pitch, roll, and azimuth.

4. FIELD TEST DATA PROCESSING

The data processing strategy is shown in Figure 7. A loose integration strategy was adopted to simplify development and to assess algorithm performance. In each reduced IMU configuration (details below), both the tactical and MEMS-grade IMUs were used. The GPS-only solution was obtained with GPS solution software (C^3NAVG^2) developed in the PLAN group at the University of Calgary. The GPS measurement update rate of the Kalman filter was 1 Hz, and the integrated solution output rate was 10 Hz.

5. GPS/REDUCED IMU EVALUATION

In order to verify the LTP method and to evaluate the performance of the GPS/reduced IMU with a local terrain predictor, a series of tests were performed using different IMU configurations. In particular, both reduced IMU configurations (3A1G and 2A1G) were tested using each grade of IMU (tactical and MEMS), for a total of four combinations. All reduced IMUs are integrated with GPS using a loose coupling strategy.

5.1. GPS/3A1G integration

Figure 8 shows the velocity and attitude errors of GPS/3A1G (HG1700) with LTP and Figure 9 is the velocity and attitude errors of GPS/3A1G (Crista) with LTP. Statistics from the two figures are shown in Table 1 and it can be seen that the RMS of the pitch and roll errors for both the HG1700 and Crista IMU are reduced to less than 0.8 degrees from the actual

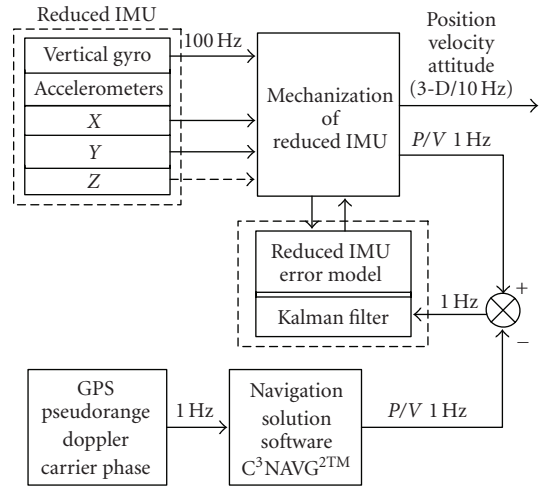

Figure 7: Data processing block diagram.

local terrain value of 2.1 degrees. This means that the LTP can help to estimate the pitch and roll, suggesting the model is valid in the GPS/3A1G case. Furthermore, comparing the performance of the HG1700 and Crista IMUs from Table 1, it can be seen that the lower grade IMU (Crista) has poorer performance. The azimuth error using the Crista is near twice that when using the HG1700. It is affected by the grade of the IMU since the azimuth is calculated from the vertical gyro measurement. But the difference in the pitch and roll errors between the two systems is small. With the HG1700 IMU, the pitch and roll errors are only reduced about 20% compared to the Crista IMU, which is not as

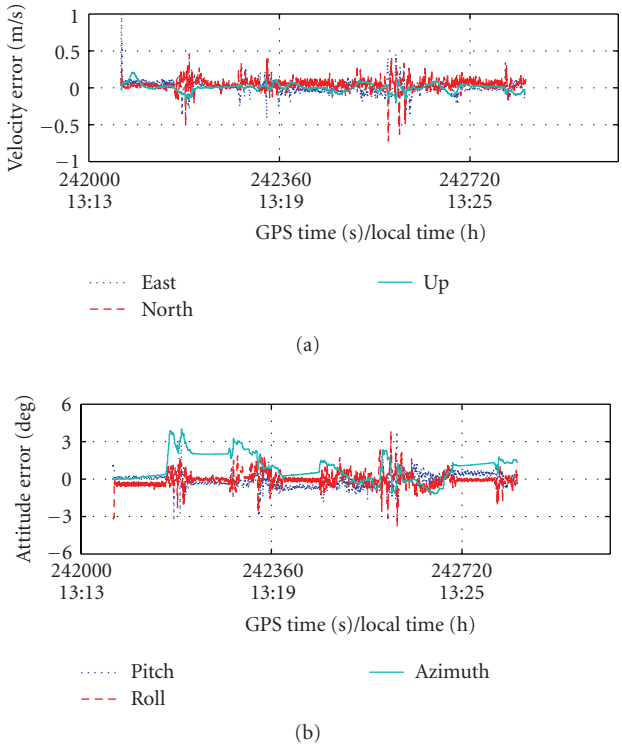

Figure 8: Velocity and attitude errors of GPS/3A1G (HG1700) with LTP.

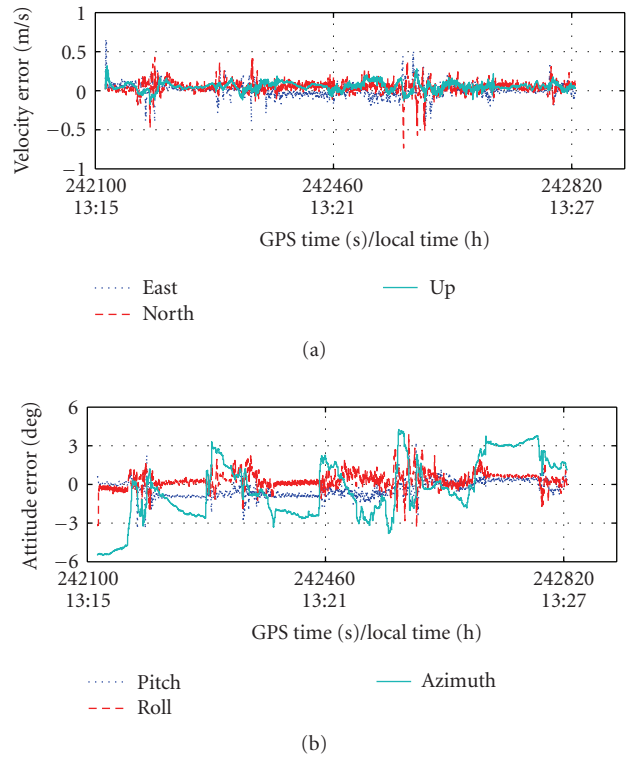

Figure 9: Velocity and attitude errors of GPS/3A1G (Crista) with LTP.

Table 1: Attitude and velocity error statistics of GPS/3A1G with LTP.

Reduced IMU	RMS of attitude error (Deg.)			RMS of velocity error (m/s)		
	Pitch	Roll	Azimuth	East	North	Up
3A1G (HG1700)	0.57	0.58	1.38	0.08	0.08	0.05
3A1G (Crista)	0.72	0.70	2.38	0.08	0.08	0.08

much as in the azimuth direction. They are affected less by the grade of the IMU since the pitch and roll of the two systems come from the same terrain model and the accuracy of the accelerometers have less effect on the pitch and roll estimation. The east and north velocity errors of the two systems are the same. The reason for this result will be given in the following paragraph. In contrast, the vertical velocity error is affected by the grade of the IMU since the vertical velocity is calculated from the vertical accelerometer measurement. Finally, from Figures 8 and 9, it can be seen that the velocity error is related to the attitude error, especially to the pitch and roll errors. When pitch and/or roll have large errors, the velocity error will increase.

In the above paragraph, it is stated that with a higher grade IMU (HG1700), although its pitch and roll estimation errors are reduced about 20% compared to the Crista IMU, its east and north velocity errors are not reduced. This may seem contradictory because reducing pitch and roll estimation errors generally reduces velocity error. The reason for this result is that although the Crista IMU has lower pitch and roll estimation accuracy, some of its pitch and roll information is "estimated out" in its horizontal accelerometer biases. So the total effect from the Crista IMU on horizontal velocity is the same with that from the HG1700. The further explanation for this result should be based on the separability of pitch, roll, and horizontal accelerometer biases. To this end, from (32), it can be seen that the cross product of the specific force and attitude errors ($\mathbf{F}^{\ell 1}\boldsymbol{\varepsilon}^{\ell 1}$) and accelerometer bias ($\mathbf{b}$) have a similar effect on velocity error and are thus coupled since $\mathbf{R}_{\ell 1}^{\ell} \approx \mathbf{R}_{b}^{\ell}$ when pitch and roll are small (only a few degrees). Since the specific force ($\mathbf{F}^{\ell 1}$) is known, it can help to separate the attitude error ($\boldsymbol{\varepsilon}^{\ell 1}$), especially for pitch and roll, and the accelerometer bias ($\mathbf{b}$), especially for horizontal accelerometer biases. But the attitude error and the accelerometer bias cannot be separated completely, and the horizontal accelerometer biases and specific force affect the pitch and roll estimation accuracy.

In fact, reducing pitch and roll estimation errors can reduce velocity error if the pitch and roll are not estimated in other variables. This is why the LTP method is presented in this paper. If only the velocity error caused by pitch, roll, and gravity acceleration is considered, the theoretical horizontal velocity errors for GPS/reduced IMU during GPS sampling period can be obtained with the following approximate equation [19]:

$$\begin{aligned} \delta v_x &= \delta r g t, \\ \delta v_y &= -\delta p g t, \end{aligned} \tag{37}$$

Table 2: Attitude and velocity error statistics of GPS/3A1G (Crista) without LTP.

Reduced IMU	RMS of attitude error (Deg.)			RMS of velocity error (m/s)		
	Pitch	Roll	Azimuth	East	North	Up
3A1G (Crista)	2.17	1.99	15.90	0.69	0.74	0.13

where δv_x and δv_y are velocity errors in the right and forward directions in b-frame, respectively, δp and δr are pitch and roll estimation errors, respectively, g is gravity acceleration, and t is time. For local terrain, if pitch and roll are not estimated, suppose $\delta p = \delta r = 2.1$ degrees, which are the original RMSs of pitch and roll, and suppose $t = 1$ s, the GPS sampling period, the horizontal velocity errors calculated from (37) are $|\delta v_x| = |\delta v_y| \approx 0.36$ m/s. In contrast, if the pitch and roll are estimated, suppose $\delta p = \delta r = 0.7$ degrees, which are the RMSs of pitch and roll errors obtained above, the horizontal velocity errors from (37) are $|\delta v_x| = |\delta v_y| \approx 0.12$ m/s. From the above calculation results, it can be seen that the pitch and roll estimation in a GPS/reduced IMU (3A1G) with an LTP can reduce velocity estimation error. This assertion is supported by the results obtained when the pitch and roll values are fixed to zero (i.e., no LTP). The corresponding results obtained using the Crista IMU are summarized in Table 2. Comparing Tables 1 and 2, it can be seen that without the LTP, the velocity error increases greatly, especially for horizontal velocities, and so does the azimuth error. This larger velocity error is caused by pitch and roll errors, and also by the larger azimuth error.

Returning to the original analysis, from Figures 8(a) and 9(a) it can be seen that there are some larger velocity errors (more than 0.5 m/s) in the GPS/reduced IMU (3A1G) with an LTP. These errors are caused by pitch and roll estimation errors. As shown in Figure 8(b), these pitch and roll estimation errors can reach more than 3 degrees. Suppose $\delta p = \delta r = 3$ degrees, and $t = 1$ s, from (37), the horizontal velocity error is calculated as $\sqrt{\delta v_x^2 + \delta v_y^2} \approx 0.73$ m/s, which is almost the same value observed in Figure 8(a). These larger pitch and roll estimation errors are caused by the local terrain variations. When pitch or/and roll changed during test, the GPS/reduced IMU with an LTP will try to track this change or to estimate the new pitch and roll value. But it needs time to track the new value or converge at the new value in estimation. Before the estimation converges to the new value, it will produce larger estimation error, which can be explained with estimation theory (e.g., [20]).

Finally, it can be concluded that the velocity error of GPS/reduced IMU with an LTP is related to local terrain variations, especially to pitch and roll variations. In order to reduce the effect of local terrain variation on the velocity error, the GPS sampling rate should be increased.

5.2. GPS/2A1G integration

In the test, as before, both HG1700 and Crista IMU were used in this configuration. The test results for both IMUs are shown in Figures 10 and 11, respectively. Their statistics are listed in Table 3.

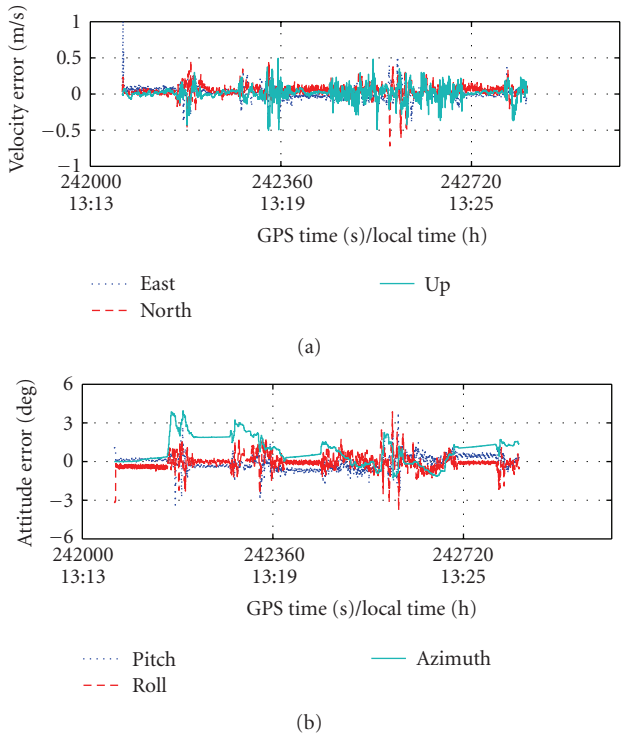

Figure 10: Velocity and attitude errors of GPS/2A1G (HG1700) with LTP.

Table 3: Attitude and velocity error statistics of GPS/2A1G with LTP.

Reduced IMU	RMS of attitude error (Deg.)			RMS of velocity error (m/s)		
	Pitch	Roll	Azimuth	East	North	Up
2A1G (HG1700)	0.57	0.59	1.35	0.08	0.08	0.09
2A1G (Crista)	0.71	0.70	2.38	0.08	0.08	0.09

From the statistics, it can be seen that the pitch and roll RMS errors for both the HG1700 and Crista IMUs are reduced greatly from the local terrain original value, just as in GPS/3A1G case. This suggests that the LTP is valid in the GPS/2A1G case as well. Further, from Table 3, it can be seen that the Crista reduced IMU has larger attitude errors than the HG1700 reduced IMU, as expected. As with the 3A1G configuration, the azimuth error of the GPS/2A1G (Crista) is almost two times that of the GPS/2A1G (HG1700) and the pitch and roll errors of the HG1700 IMU are only reduced about 20% compared to the Crista IMU for the same reasons as before. From Table 3, it also can be seen that the two grades of IMUs have the same velocity error. For the east and north velocity errors, the reason for this result is the same as with the 3A1G configuration. But for the vertical velocity error, the reason is that the vertical accelerations for both grades of IMUs are calculated from the same formula as in the 2A1G configuration, which has no vertical accelerometer (and thus

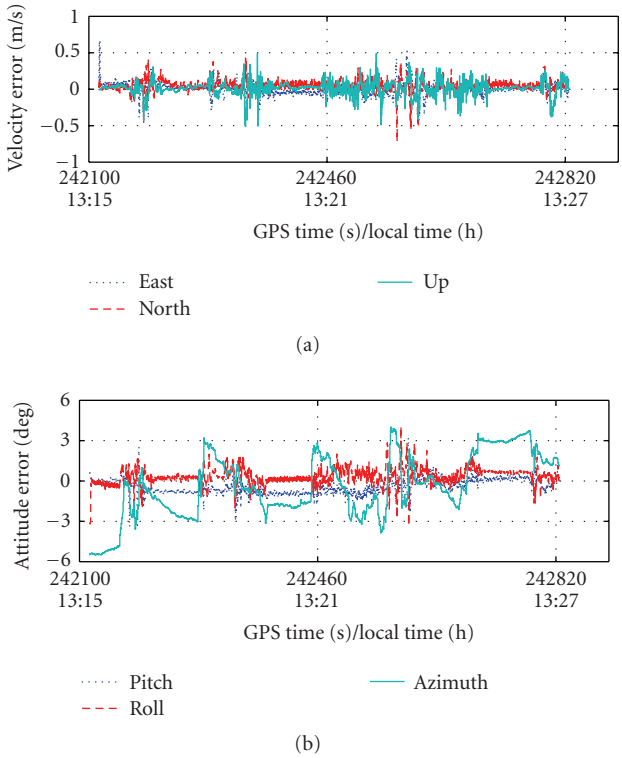

Figure 11: Velocity and attitude errors of GPS/2A1G (Crista) with LTP.

Table 4: Attitude and velocity error statistics of GPS/2A1G (Crista) without LTP.

Reduced IMU	RMS of attitude error (Deg.)			RMS of velocity error (m/s)		
	Pitch	Roll	Azimuth	East	North	Up
2A1G (Crista)	2.17	1.99	15.90	0.69	0.74	0.09

is not a function of IMU quality). Finally, from Figures 10 and 11, it can be seen that velocity error is related to attitude error, as in the 3A1G configuration.

As above, the GPS/2A1G (Crista) configuration with the pitch and roll values fixed to zero was also tested. The results are summarized in Table 4. Comparing with Table 3, it can be seen that without the estimation of pitch and roll, the velocity error and azimuth error increase greatly, just as in the GPS/3A1G case.

5.3. Comparison of GPS/3A1G and GPS/2A1G

In order to facilitate the performance comparison for the two configurations, the above results are summarized in Table 5.

From Table 5, it can be seen that the two configurations (3A1G and 2A1G) have almost the same attitude result for a certain grade of IMU. It is concluded, therefore, that, for the datasets considered here, the reduced IMU configuration has little effect on the attitude performance of the GPS/reduced IMU. This is because the attitude estimation in the GPS/reduced IMU is mainly determined by GPS,

Table 5: Attitude and velocity error statistics of GPS/reduced IMU with LTP.

Reduced IMU	RMS of attitude error (Deg.)			RMS of velocity error (m/s)		
	Pitch	Roll	Azimuth	East	North	Up
3A1G (HG1700)	0.57	0.58	1.38	0.08	0.08	0.05
2A1G (HG1700)	0.57	0.59	1.35	0.08	0.08	0.09
3A1G (Crista)	0.72	0.70	2.38	0.08	0.08	0.08
2A1G (Crista)	0.71	0.70	2.38	0.08	0.08	0.09

horizontal accelerometer biases, local terrain, and the vertical gyro measurement. Vertical accelerometer has no direct effect on the attitude estimation. For velocity error, Table 5 shows that two IMU configurations have the same east and north velocity errors, but the 3A1G configuration has a smaller vertical velocity error. This means that the horizontal velocity errors are not affected by the configuration or the vertical accelerometer, but the vertical velocity error is affected by the configuration because the vertical velocity is calculated directly from vertical acceleration. From the above analysis, it can be concluded that the vertical accelerometer in a reduced IMU only can mitigate some vertical velocity error, but cannot reduce other velocity and attitude errors. Therefore, the 2A1G configuration is a reasonable choice for vehicular applications when the tradeoff between cost and performance is considered.

6. GPS OUTAGE TEST

To assess the performance of the GPS/reduced IMU system with an LTP during GPS outage, a series of GPS outage tests were conducted.

6.1. Test description

In the outage tests, both grades of IMU and both reduced IMU configurations were used. Ten 30 seconds long GPS outages were simulated in the data by artificially omitting the satellites during postmission processing. These outages are carefully selected to represent varying vehicle dynamics, as shown in Figure 12. In the outage tests, GPS/reduced IMU with an LTP means that the pitch and roll estimates are almost constant value during GPS outage (they vary slightly because of the first-order Gauss-Markov process model with long correlation time (500 seconds) used); GPS/reduced IMU without an LTP means that the pitch and roll estimates are chosen as zero during GPS outage. In the tests, the RMS of position or velocity error is calculated from the following equation:

$$\mathrm{RMS}(t_i) = \sqrt{\frac{1}{10}\sum_{j=1}^{10}\left(x_j(t_i) - x_r(t_i)\right)^2}, \tag{38}$$

where t_i is GPS outage duration (from 0 to 30 seconds), $x_j(t_i)$ is the output of reduced IMU in the jth GPS outage at t_i, and $x_r(t_i)$ is the reference solution at t_i.

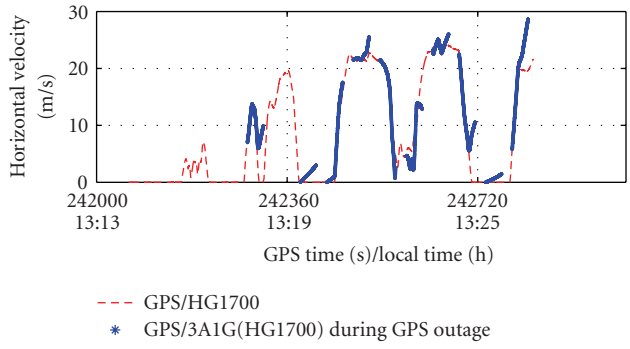

Figure 12: Ten 30 seconds GPS outage gaps.

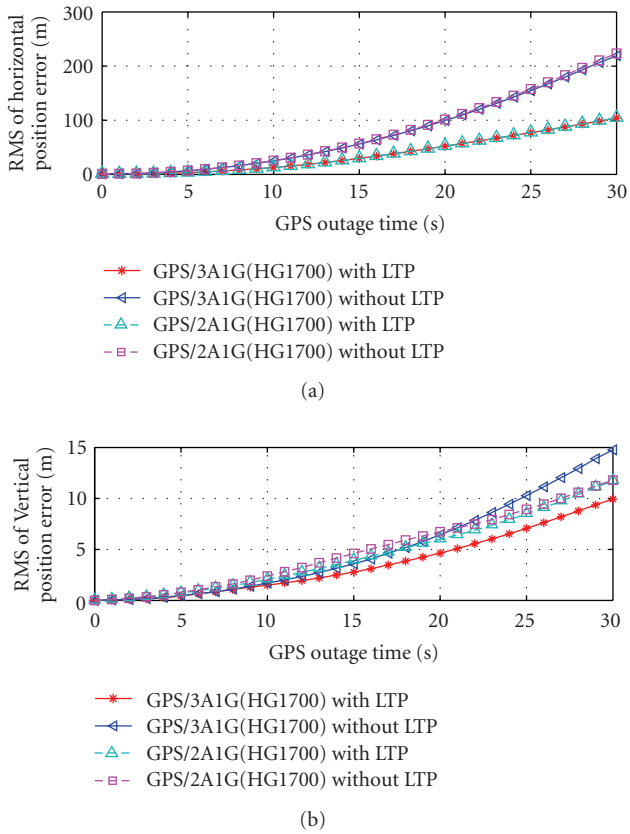

Figure 13: Horizontal and vertical position error comparison between GPS/reduced IMU (HG1700) with and without LTP.

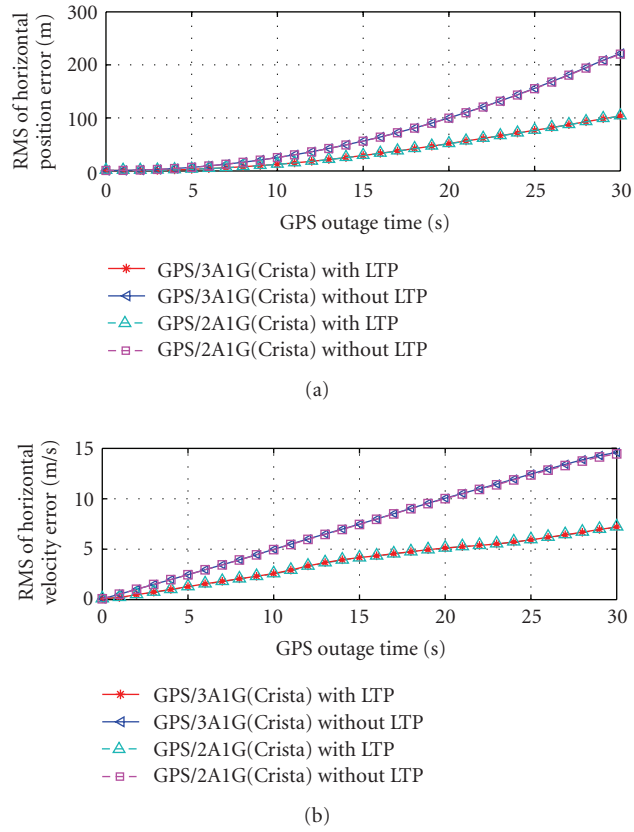

Figure 14: Horizontal position and velocity error comparison between GPS/reduced IMU (Crista) with and without LTP.

Table 6: Horizontal and vertical position error comparison between GPS/reduced IMU with and without LTP at the end of GPS outage.

Reduced IMU	RMS of position error (m)			
	Horizontal		Vertical	
	LTP	No LTP	LTP	No LTP
3A1G (HG1700)	104	219	10	15
2A1G (HG1700)	104	223	12	12
3A1G (Crista)	103	221	11	12
2A1G (Crista)	103	220	11	12

6.2. Results

The position and velocity RMS errors as a function of time since the last GPS measurement are shown in Figures 13, 14, and 15, and the results at the end of GPS outage are summarized in Table 6. For the vertical position, since the GPS/reduced IMU has a larger bias (about 4 m) from GPS compared to the reference solution, in order to facilitate the analysis, this bias is removed when calculating the RMS of the vertical position with (38). If this bias is not removed in the RMS calculation, the result for the Crista IMU is shown in Figure 16.

6.3. Analysis

From Table 6, it can be seen that, for the GPS/reduced IMU without an LTP, the horizontal position errors for different grades of IMU (HG1700 and Crista) and different reduced IMU configurations (3A1G and 2A1G) are almost the same, from 219 to 223 m, since the horizontal position error is mainly determined by the local terrain when there is no LTP used during GPS outage. During a GPS outage, if only the position error caused by pitch, roll, and gravity acceleration is considered, the theoretical horizontal position errors for the GPS/reduced IMU without an LTP can be obtained with

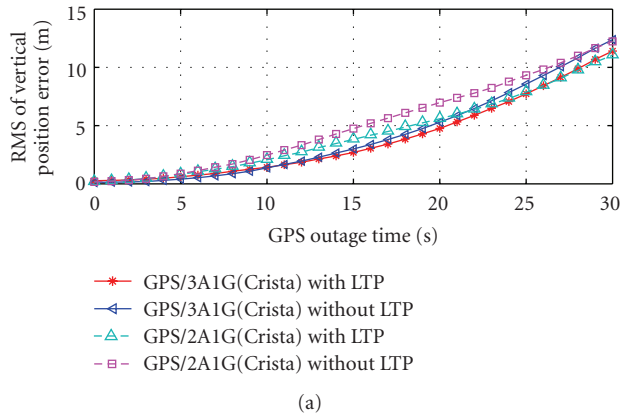

(a)

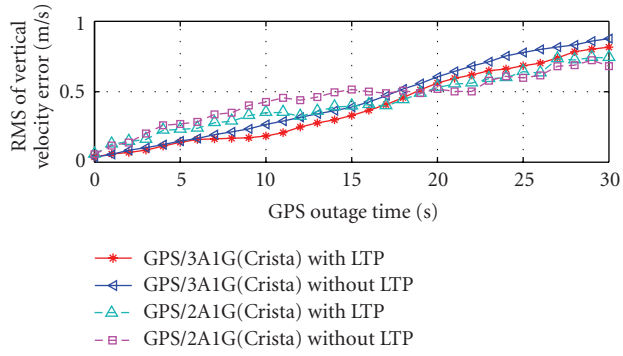

(b)

Figure 15: Vertical position and velocity error comparison between GPS/reduced IMU (Crista) with and without LTP.

the following approximate equation derived by integrating (37):

$$\delta x = \frac{1}{2}\delta r g t^2, \qquad \delta y = -\frac{1}{2}\delta p g t^2, \tag{39}$$

where δx and δy are position errors in the right and forward directions, respectively, in the b-frame, δp and δr are pitch and roll estimation errors, respectively, g is gravity acceleration, and t is time. For local terrain, the RMS of the actual pitch and roll are all about 2.1 degrees. The GPS outage duration is 30 seconds. Suppose $\delta p = \delta r = 2.1$ degrees, and $t = 30$ seconds, the position errors in the right and forward directions can be calculated from (39) to be $|\delta x| = |\delta y| \approx 162$ m. Then the RMS of the horizontal position error is $162\sqrt{2} \approx 229$ m. So the outage test results and theoretical results are very close.

With an LTP, the horizontal position errors for different IMU grades and different configurations are reduced greatly, as shown in Figures 13(a) and 14(a) and Table 6. From Table 6, it can be seen that with an LTP, even though the grade and configuration of the reduced IMUs are different, they have similar results; the RMSs of the horizontal position errors for all IMUs and configurations are almost the same, from 103 to 104 m, which is less than half the error without an LPT.

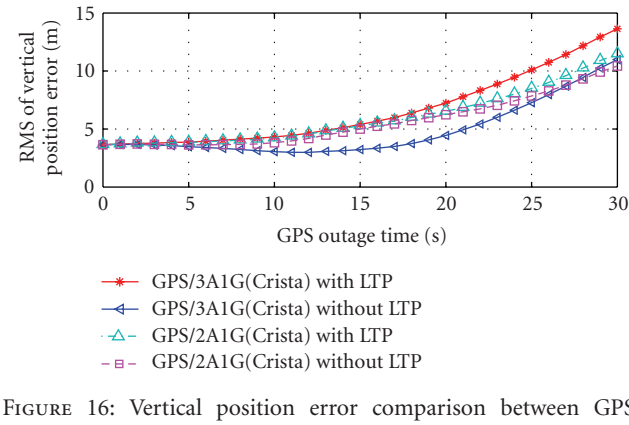

Figure 16: Vertical position error comparison between GPS/reduced IMU (Crista) with and without LTP When the vertical position bias of GPS/reduced IMU is not removed in RMS calculation.

The explanation for this result is that the position error of the GPS/reduced IMU with an LTP is also affected by the local terrain during GPS outages because it is impossible to predict the local terrain accurately when there is no other external information. When GPS is unavailable, the only thing that can be used for pitch and roll estimation is the previous estimates of pitch and roll. In order to use the previous estimates of pitch and roll in the GPS outage, the correlation times of the pitch and roll models are chosen to be large. If the pitch and roll changed during the GPS outage, it will introduce more position errors. In fact, during GPS outages, the horizontal position error comes from two parts: the first is produced by the initial pitch and roll errors; the second is produced by the pitch and roll change during a GPS outage.

Figure 14(b) shows that for the Crista IMU under both configurations, the horizontal velocity error of the GPS/reduced IMU with an LTP is about half that of the GPS/reduced IMU without an LTP. It further demonstrates that the LTP is valid in a GPS/reduced IMU during GPS outage.

Figure 13(b) shows the vertical position errors of two configurations of the GPS/reduced IMU (HG1700) with and without an LTP. Figure 15(a) shows the vertical position errors of two configurations of a GPS/reduced IMU (Crista) with and without an LTP. Their statistics are listed in Table 6 and it can be seen that the vertical position error is reduced only slightly, if at all, with an LTP. For the vertical position error, if only the position error caused by pitch, roll, and gravity acceleration is considered, its approximate formula can be derived from (34) and is as follows:

$$\begin{aligned}\delta z &= \frac{1}{2}g(\cos p \cos r - \cos \hat{p} \cos \hat{r})t^2 \\ &\approx -\frac{1}{4}g\left((p+\hat{p})\delta p + (r+\hat{r})\delta r\right)t^2,\end{aligned} \tag{40}$$

where p is pitch, r is roll, $\delta p = p - \hat{p}$, $\delta r = r - \hat{r}$, g is gravity acceleration, and t is time. For the local terrain, the RMSs of its original pitch and roll are about 2.1 degrees, suppose $p = r = 2.1$ degrees, $\hat{p} = \hat{r} = 0$, so $\delta p = \delta r = 2.1$ degrees,

and suppose the outage duration $t = 30$ seconds, from (40), the vertical position error can be calculated as $|\delta z| = 5.9$ m; when the RMSs of pitch and roll errors are about 0.7 degrees, suppose $p = r = 2.1$ degrees, $\hat{p} = \hat{r} = 1.4$ degrees, and $\delta p = \delta r = 0.7$ degrees, the vertical position error is calculated as $|\delta z| = 3.3$ m. Comparing the theoretical results and outage test results (in Table 6), it can be seen that the test results are larger. The reasons for this are as follows. First, during a GPS outage, the pitch and roll changes. Second, since the vertical position error is small, other factors, which can also cause vertical position error, need to be considered such as the vertical projection of the vehicle's acceleration and the cross product of the pitch angular velocity and the vehicle's velocity. All the above factors will accumulate the vertical position error. From Table 6, it also can be seen that the vertical position errors are almost the same as for different grades of IMUs and different configurations. This is because the vertical position error depends largely on the local terrain, and it is not significantly affected by the grade of IMU or the configuration.

The vertical velocity errors of the GPS/reduced IMU (Crista) are shown in Figure 15(b). From Figure 15(b), it can be seen that the vertical velocity error is reduced only marginally or remains the same with an LTP, just like the vertical position error. The explanation for this result is the same as that for vertical position error. However, if the vertical position bias of the GPS/reduced IMU (Crista) is not removed in the RMS calculation, the result shown in Figure 16 does not show a consistent relationship with the vertical velocity error shown in Figure 15(b).

7. SUMMARY AND CONCLUSIONS

This paper presents a local terrain predictor (LTP) for reduced IMU in land vehicle navigation. Based on the LTP, the navigation equations and error model of the reduced IMU are established. Then GPS/reduced IMU with an LTP is introduced. To verify the LTP and investigate the performance of GPS/reduced IMU with an LTP, a field vehicle test was conduced to collect GPS and IMU data for integration tests. In the field test, two grades of IMUs were used: a tactical-grade IMU (Honeywell HG1700), and an MEMS-grade IMU (Crista). After the data collection, a series of system configuration tests were conducted to verify the new method. In these tests, two kinds of reduced IMU configurations were used: three accelerometers plus one vertical gyro (3A1G) and two horizontal accelerometers plus one vertical gyro (2A1G). Test results show that higher grade IMU has higher accuracy of attitude estimation, especially for azimuth; two grade IMUs have the same horizontal velocity errors; two configurations have almost the same attitude error, and have the same horizontal velocity errors, but 3A1G configuration has smaller vertical velocity error and higher accuracy vertical accelerometer has smaller vertical velocity error; 2A1G configuration for different grade IMU has the same vertical velocity error; velocity error is related to local terrain variations. Based on the above results, the following conclusions are drawn:

(1) with an LTP, pitch and roll can be estimated, and velocity error can be reduced, especially for horizontal velocity error, it can be reduced by more than 80% compared to without LTP;

(2) 2A1G is the better configuration when cost and performance are considered.

Following the system configuration tests, some GPS outage tests were conducted. In this case, ten 30 seconds GPS gaps were simulated. Two conclusions are drawn from the following results

(1) the LTP is valid, and can reduce position and velocity error during GPS outage;

(2) with an LTP, the horizontal position and velocity errors of different grade IMUs and different configurations are reduced greatly, but the vertical position and velocity errors are reduced only a little bit or kept the same value.

In conclusion, LTP is a valid attitude error model (for pitch and roll) for reduced IMU, and can improve the navigation performance of GPS/reduced IMU. Tests confirm that the LTP can provide better navigation performance in areas with limited terrain variation. The algorithms are, however, applicable to more variable terrain but the expected improvement may degrade. This will be investigated in later work.

APPENDIX

A. MECHANIZATION OF FULL SET IMU

Since the navigation equations and error model of full set IMU can be used to derivate the equations for a reduced IMU, they are briefly introduced in the following.

A.1. Navigation equations of full set IMU

The equations of motion for a full IMU are given by [13, 19]

$$\begin{aligned}\dot{\mathbf{r}}^{\ell} &= \mathbf{D}^{-1}\mathbf{v}^{\ell},\\ \dot{\mathbf{v}}^{\ell} &= \mathbf{R}_b^{\ell}\mathbf{f}^b - (2\boldsymbol{\Omega}_{ie}^{\ell} + \boldsymbol{\Omega}_{e\ell}^{\ell})\mathbf{v}^{\ell} + \mathbf{g}^{\ell},\\ \dot{\mathbf{R}}_b^{\ell} &= \mathbf{R}_b^{\ell}(\boldsymbol{\Omega}_{ib}^{b} - \boldsymbol{\Omega}_{i\ell}^{b}),\end{aligned} \tag{A.1}$$

where $\boldsymbol{\Omega}_{ie}^{\ell} = [\boldsymbol{\omega}_{ie}^{\ell}\times]$, $\boldsymbol{\Omega}_{e\ell}^{\ell} = [\boldsymbol{\omega}_{e\ell}^{\ell}\times]$, $\boldsymbol{\Omega}_{ib}^{b} = [\boldsymbol{\omega}_{ib}^{b}\times]$, $\boldsymbol{\Omega}_{i\ell}^{b} = [\boldsymbol{\omega}_{i\ell}^{b}\times]$ and $\boldsymbol{\Omega}_{xy}^{a} = [\boldsymbol{\omega}_{xy}^{a}\times]$ are skew symmetric matrices, where $\boldsymbol{\omega}_{xy}^{a}$ is a rotation rate column vector, from y-frame to x-frame, and the vector is in a-frame. $\mathbf{f}^b = [f_x^b \;\; f_y^b \;\; f_z^b]^T$ is the measurement of accelerometers, $\boldsymbol{\omega}_{ib}^{b} = (\omega_{ibx}^{b} \;\; \omega_{iby}^{b} \;\; \omega_{ibz}^{b})^T$ is the measurement of gyros. $\mathbf{r}^{\ell} = [\varphi \;\; \lambda \;\; h]^T$ is position, φ is latitude, λ is longitude, h is height. $\mathbf{v}^{\ell} = [v_e \;\; v_n \;\; v_u]^T$ is velocity, v_e is velocity in east, v_n is velocity in north, and v_u is in up. $\mathbf{D}^{-1}$ is a matrix, which transfers velocity in ℓ-frame into position variation rate in ℓ-frame. In b-frame, x points right, y points forward, and z points up. In ℓ-frame, e is east,

n is north, u is up. $\mathbf{g}^{\ell} = [0 \;\; 0 \;\; -g]^{T}$, g is the acceleration of gravity. $\mathbf{R}_{b}^{\ell}$ is a direction cosine matrix, from b-frame to ℓ-frame.

A.2. Corresponding error model of full set IMU

The error model of a full set IMU is given by [13, 19]

$$\begin{bmatrix} \delta\dot{\mathbf{r}}^{\ell} \\ \delta\dot{\mathbf{v}}^{\ell} \\ \dot{\boldsymbol{\varepsilon}}^{\ell} \\ \dot{\mathbf{d}} \\ \dot{\mathbf{b}} \end{bmatrix} = \begin{bmatrix} \mathbf{0}_{3\times3} & \mathbf{D}^{-1} & \mathbf{0}_{3\times3} & \mathbf{0}_{3\times3} & \mathbf{0}_{3\times3} \\ \mathbf{0}_{3\times3} & \mathbf{B} & -\mathbf{F}^{\ell} & \mathbf{0}_{3\times3} & \mathbf{R}_{b}^{\ell} \\ \mathbf{0}_{3\times3} & \mathbf{Q} & -\boldsymbol{\Omega}_{i\ell}^{\ell} & \mathbf{R}_{b}^{\ell} & \mathbf{0}_{3\times3} \\ \mathbf{0}_{3\times3} & \mathbf{0}_{3\times3} & \mathbf{0}_{3\times3} & -\boldsymbol{\Gamma} & \mathbf{0}_{3\times3} \\ \mathbf{0}_{3\times3} & \mathbf{0}_{3\times3} & \mathbf{0}_{3\times3} & \mathbf{0}_{3\times3} & -\boldsymbol{\Lambda} \end{bmatrix} \begin{bmatrix} \delta\mathbf{r}^{\ell} \\ \delta\mathbf{v}^{\ell} \\ \boldsymbol{\varepsilon}^{\ell} \\ \mathbf{d} \\ \mathbf{b} \end{bmatrix} + \begin{bmatrix} \mathbf{0}_{3\times1} \\ \mathbf{0}_{3\times1} \\ \mathbf{0}_{3\times1} \\ \mathbf{W}_{d} \\ \mathbf{W}_{b} \end{bmatrix}, \tag{A.2}$$

where $\delta\mathbf{r}^{\ell} = [\delta\varphi \;\; \delta\lambda \;\; \delta h]^{T}$ is position error, $\delta\mathbf{v}^{\ell} = [\delta v_e \;\; \delta v_n \;\; \delta v_u]^{T}$ is velocity error, $\boldsymbol{\varepsilon}^{\ell} = [\varepsilon_x^{\ell} \;\; \varepsilon_y^{\ell} \;\; \varepsilon_z^{\ell}]^{T}$ is attitude error in ℓ-frame, $\mathbf{d} = [d_x \;\; d_y \;\; d_z]^{T}$ is gyro drift in b-frame, $\mathbf{b} = [b_x \;\; b_y \;\; b_z]^{T}$ is accelerometer bias in b-frame, $\boldsymbol{\Omega}_{i\ell}^{\ell} = [\boldsymbol{\omega}_{i\ell}^{\ell}\times]$. $\mathbf{B}$ is a matrix, which transfers velocity error into velocity error varying rate in ℓ-frame. $\mathbf{Q}$ is a matrix that transfers velocity error into attitude error rate in ℓ-frame. $\mathbf{F}^{\ell} = [\mathbf{f}^{\ell}\times]$, $\mathbf{f}^{\ell} = [f_e \;\; f_n \;\; f_u]^{T}$, $\boldsymbol{\Gamma} = \mathrm{diag}(\alpha_x \;\; \alpha_y \;\; \alpha_z)$, $\boldsymbol{\Lambda} = \mathrm{diag}(\beta_x \;\; \beta_y \;\; \beta_z)$, $\mathbf{0}_{3\times3}$ is a zero matrix with dimension 3×3, $\mathbf{0}_{3\times1}$ is a zero vector with dimension 3×1. $\mathbf{W}_d$ and $\mathbf{W}_b$ are driving noise. Other variables and parameters are the same with those in (A.1).

The above error model is a simplified model. The terms related to position error in position, velocity and attitude error equations are ignored because they are very small. The white noise terms of accelerometer's error and gyro's error, which are added to velocity error equation and attitude error equation, respectively, are also ignored in order to simplify the derivation of the equations for a reduced IMU.

ACKNOWLEDGMENT

The authors would like to acknowledge Dr. O' Driscoll and Tao Li for their support during the field test.

REFERENCES

[1] X. Niu, S. Nassar, and N. El-Sheimy, "An accurate land-vehicle MEMS IMU/GPS navigation system using 3D auxiliary velocity updates," *Navigation*, vol. 54, no. 3, pp. 177–188, 2007.

[2] M. Spangenberg, V. Calmettes, D. Kubrak, and O. Julien, "Optimized low-cost HSGPS/IMU/WSS land vehicle navigation system for urban navigation," in *Proceedings of the 20th International Technical Meeting of the Satellite Division of the Institute of Navigation (ION GNSS '07)*, pp. 70–78, U.S. Institute of Navigation, Fort Worth Tex, USA, September 2007.

[3] J. Gao, M. G. Petovello, and M. E. Cannon, "Development of precise GPS/INS/wheel speed sensor/yaw rate sensor integrated vehicular positioning system," in *Proceedings of the National Technical Meeting of the Institute of Navigation (ION NTM '06)*, vol. 2, pp. 780–792, U.S. Institute of Navigation, Monterey, Calif, USA, January 2006.

[4] S. Godha and M. E. Cannon, "Integration of DGPS with a low cost MEMS—based Inertial Measurement Unit (IMU) for land vehicle navigation application," in *Proceedings of the 18th International Technical Meeting of the Satellite Division of the Institute of Navigation (ION GNSS '05)*, pp. 333–345, U.S. Institute of Navigation, Long Beach, Calif, USA, September 2005.

[5] Z. Syed, P. Aggarwal, X. Niu, and N. El-Sheimy, "Economical and robust inertial sensor configuration for a portable navigation system," in *Proceedings of the 20th International Technical Meeting of the Satellite Division of the Institute of Navigation (ION GNSS '07)*, pp. 2129–2135, U.S. Institute of Navigation, Fort Worth Tex, USA, September 2007.

[6] X. Niu, S. Nasser, C. Goodall, and N. El-Sheimy, "A universal approach for processing any MEMS inertial sensor configuration for land-vehicle navigation," *The Journal of Navigation*, vol. 60, no. 2, pp. 233–245, 2007.

[7] B. Phuyal, "An experiment for a 2-D and 3-D GPS/INS configuration for land vehicle applications," in *Position Location and Navigation Symposium (PLANS '04)*, pp. 148–152, Monterey, Calif, USA, April 2004.

[8] W. Ochieng, J. W. Polak, R. B. Noland, et al., "Integration of GPS and dead reckoning for real-time vehicle performance and emissions monitoring," *GPS Solutions*, vol. 6, no. 4, pp. 229–241, 2003.

[9] A. Brandit and J. F. Gardner, "Constrained navigation algorithms for strapdown inertial navigation systems with reduced set of sensors," in *Proceedings of the American Control Conference (ACC '98)*, vol. 3, pp. 1848–1852, Philadelphia, Pa, USA, June 1998.

[10] P. Daum, J. Beyer, and T. F. W. Köhler, "Aided inertial land navigation system (ILANA) with a minimum set of inertial sensors," in *Position Location and Navigation Symposium (PLANS '94)*, pp. 284–291, Las Vegas, Nev, USA, April 1994.

[11] C. Vlcek, P. McLain, and M. Murphy, "GPS/dead reckoning for vehicle tracking in the 'urban canyon' environment," in *Proceedings of the IEEE-IEE Vehicle Navigation and Informations Systems Conference (VNIS '93)*, pp. A34–A37, Ottawa, Canada, October 1993.

[12] M. G. Petovello, *Real-time integration of a tactical-grade IMU and GPS for high-accuracy position and navigation*, Ph.D. dissertation, Department of Geomatics Engineering, University of Calgary, Calgary, Canada, 2003.

[13] D. Titterton and J. Weston, *Strapdown Inertial Navigation Technology*, The Institution of Electrical Engineers, London, UK, 2nd edition, 2004.

[14] J. Farrell and M. Barth, *The Global Positioning System & Inertial Navigation*, McGraw-Hill, New York, NY, USA, 1999.

[15] J. Kuchar, "Markov model of terrain for evaluation of ground proximity warning system thresholds," *Journal of Guidance, Control, and Dynamics*, vol. 24, no. 3, pp. 428–435, 2001.

[16] C. Jekeli, *Inertial Navigation Systems with Geodetic Applications*, Walter de Gruyter, New York, NY, USA, 2001.

[17] Cloud Cap Technology, "Crista Inertial Measurement Unit (IMU) Interface/Operation Document," Cloud Cap Technology Inc., USA, March 2006, http://www.cloudcaptech.com/.

[18] S. Godha, *Performance evaluation of low cost MEMS-based IMU integrated with GPS for land vehicle navigation application*, M.S. thesis, Department of Geomatics Engineering, University of Calgary, Calgary, Canada, 2006.

[19] N. El-Sheimy, "Inertial Techniques and INS/DGPS Integration," ENGO699.64 Course Notes, Department of Geomatics Engineering, University of Calgary, Canada, Section two, 2007.

[20] A. Gelb, *Applied Optimal Estimation*, The MIT Press, Cambridge, Mass, USA, 1974.